COMMUNICATION

# A Selenophene-Containing Conjugated Organic Ligand for Two-Dimensional Halide Perovskite

Received 00th January 20xx,
Accepted 00th January 20xx

DOI: 10.1039/x0xx00000x

Zitang Wei,[a] Kang Wang,[a] Wenchao Zhao,[a] Yao Gao,[a] Qixuan Hu,[a] Ke Chen,[b] and Letian Dou*[a]

**A selenophene-containing conjugated organic ligand 2-(4'-methyl-5'-(5-(3-methylthiophen-2-yl)selenophen-2-yl)-[2,2'-bithiophen]-5-yl)ethan-1-aminium (STm) is synthesized and incorporated into Sn(II)-based two-dimensional perovskites, $(STm)_2SnI_4$. By introducing the STm ligand, the band offset between perovskite and ligand can be fine-tuned. Both field-effect transistor and light-emitting diode devices based on $(STm)_2SnI_4$ films exhibit high performance and enhanced operational stability.**

Organic-inorganic hybrid perovskites have gained considerable attention in semiconducting material design and optoelectronic device applications.[1-6] Commonly-used three-dimensional (3D) perovskites suffer from poor stability, which restricts their practical applications.[7, 8] Instead, two-dimensional (2D) halide perovskites were proved to have significantly improved ambient stability and reduced ion migration due to the use of bulky and hydrophobic organic ligands.[9-14] Insulating aliphatic organic ligands were initially introduced to 2D perovskites, but their wide band gaps and poor charge transport properties hindered the utilization of those 2D perovskites into optoelectronic devices.[15] Previous studies have introduced semi-conducting π-conjugated cations based on triple bonds, thiophenes, and phenyl rings into 2D perovskites to enhance the charge transport properties.[16-19] Recently, our group designed and synthesized a series of oligothiophene-based monoammonium ligands and successfully incorporated them into 2D perovskites.[20] The energy and charge transfer between organic and inorganic layers can be tuned via molecular design. Among those ligands, a quaterthiophene derivative cation, 2-(3‴,4'-dimethyl-[2,2':5',2'':5'',2‴-quaterthiophen]-5-yl)ethan-1-ammonium (namely 4Tm ligand) showed a great promise and was incorporated into Sn(II)-based 2D halide perovskite, $(4Tm)_2SnI_4$, which exhibited improved charge transport and ambient stability compared with widely-used $(C_6H_5C_2H_4NH_3)_2SnI_4$ ( or simply $(PEA)_2SnI_4$) perovskite.[21] For example, field-effect transistor (FET) devices based on $(4Tm)_2SnI_4$ exhibited a hole mobility of 2.32 $cm^2V^{-1}s^{-1}$ and light-emitting diode (LED) based on this material exhibited an external quantum efficiency (EQE) of 1.58%.[22]

The design and synthesis of 4Tm ligand demonstrated an example of incorporating heterocycles containing building blocks into perovskites. However, a relatively large energy barrier height of 4Tm ligand to $[SnI_4]^{2-}$ for charge injection may be an important factor limiting the FET and LED device performances.[21, 22] Therefore, fine-tuning the band gaps of organic ligands in 2D perovskites could be a promising strategy for perovskite materials design. In the organic electronics research field, selenophenes have been used to replace the thiophene unit to tune the highest occupied molecular orbital (HOMO), lowest unoccupied molecular orbital (LUMO) energy levels, and the band gaps of organic semiconductor materials.[23-25] Specifically, selenophene-based low-bandgap conjugated polymers have been applied to organic FETs and solar cells, which exhibited improved performances compared with the thiophene-based counterparts due to optimized band alignment.[26-28] Compared with sulphur, selenium has a bigger and looser outmost electron cloud, which can help improve orbital overlap and the charge carrier mobility.[29] Therefore, replacing thiophene with selenophene unit in the ligand design can be a promising ways to further reduce the barrier height of charge transport, which is beneficial for optoelectronic device applications.

Herein, inspired by the prior work from organic electronic community, a novel selenophene-containing conjugated organic ligand 2-(4'-methyl-5'-(5-(3-methylthiophen-2-yl)selenophen-2-yl)-[2,2'-bithiophen]-5-yl)ethan-1-aminium (STm) is designed and synthesized for 2D halide perovskites. Specifically, the third thiophene ring of the 4Tm backbone was swapped by a selenophene ring via a few simple steps (Fig. 1a). The STm ligand was then incorporated into Sn (II)-based 2D perovskite. The introduction of selenophene helps reduce the band gap of the ligand by increasing the HOMO energy level and leads to improved charge transport properties. On this basis, both FET and LED devices were fabricated based on $(STm)_2SnI_4$ thin films. Notably, the LED device achieved an

[a] Davidson School of Chemical Engineering, Purdue University, West Lafayette, IN 47907, USA.
E-mail: dou10@purdue.edu
[b] Department of Chemistry, Purdue University, West Lafayette, IN 47907, USA.
Electronic Supplementary Information (ESI) available: [details of any supplementary information available should be included here]. See DOI: 10.1039/x0xx00000x

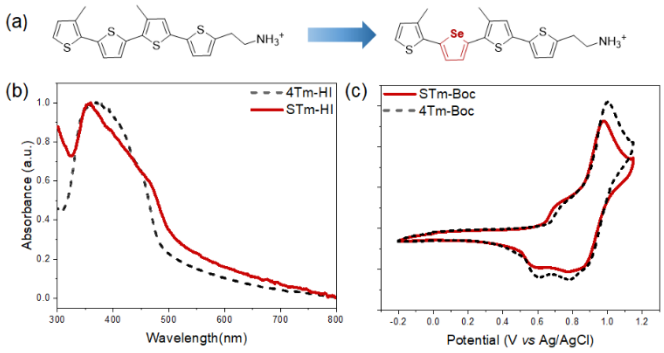


**Fig. 1** (a) Chemical structures of STm and 4Tm organic ligands. (b) UV-vis absorption and (c) cyclic voltammetry of STm and 4Tm organic ligands.

EQE of 2.28%, which has a 44% enhancement compared with $(4Tm)_2SnI_4$ LED devices.

Fig. 1a shows the chemical structure of the STm ligand. Starting from selenophene, a thiophene-selenophene-thiophene trimer was obtained via a Stille coupling reaction; then the trimer was coupled with another thiophene ring with a Boc-protected amine; finally, the iodide salt of STm-HI was obtained by removing the Boc group using HI (see methods in the ESI). Similar to the 4Tm ligand, two methyl groups were incorporated on the second and fourth thiophene units to reduce the intermolecular π- π interactions and self-aggregation. According to UV-vis absorption and cyclic voltammetry (Fig. 1b and 1c), STm ligand shows an increased HOMO energy level of -5.05 eV and a smaller optical bandgap of 2.40 eV than those of 4Tm ligand (HOMO energy level of -5.12 eV and optical bandgap of 2.49 eV).

To understand the ligand-perovskite interactions, the new conjugated STm ligand was incorporated into the 2D perovskite thin films. A spin-coating method was used to fabricate the thin films of $(STm)_2SnI_4$ and benchmark material $(4Tm)_2SnI_4$. The X-ray diffraction (XRD) pattern of $(STm)_2SnI_4$ (Fig. 2a) clearly showed a series of sharp and high-intensity diffraction peaks, confirming its layered 2D perovskite structure with the inter-layer distance calculated to be 32.0 Å, which matches the interlayer distance of the reported value of $(4Tm)_2SnI_4$ perovskite thin film (31.9 Å).[21] Note, single crystal structure of $(STm)_2SnI_4$ has not been resolved due to difficulty in obtaining high quality crystals. UV-vis absorption spectra of $(STm)_2SnI_4$ and $(4Tm)_2SnI_4$ exhibit similar optical band gaps and sharp excitonic peaks. (Fig. 2b). The optical image of $(STm)_2SnI_4$ shows a uniform film (Fig S2) with complete surface coverage and the corresponding photoluminescence (PL) image shows intensive red emission (Fig. S2) with sharp peak centred at 630 nm, which is almost identical to that of $(4Tm)_2SnI_4$ (Fig. 2c). The PL emission peak in the range from 600 nm to 700 nm comes from $[SnI_4]^{2-}$ layer, while the absence of PL from the organic ligand $STm^+$ (Fig. S1) is due to the energy transfer from organic ligands to the inorganic layers.

Based on the cyclic voltammetry profile, optical absorption, and PL emission spectra of the ligands and the corresponding perovskite thin films, the schematic of relative band alignment of STm ligand, 4Tm ligand and $[SnI_4]^{2-}$ layer was generated. (Fig. 2d) The schematic indicates a clear formation of a type-I hybrid quantum well configuration. Type-I configuration can help promote exciton confinement in $[SnI_4]^{2-}$ octahedron layer for radiative recombination, making $(STm)_2SnI_4$ suitable for efficient light-emitting applications. The band alignment also points out that the HOMO energy level of STm ligand (-5.05 eV) is closer to the valence band maximum (-5.0 eV) of $[SnI_4]^{2-}$ octahedron than that of 4Tm ligand (-5.12 eV), which could facilitate charge carrier injection between organic ligands and inorganic layers.

It is known that Sn (II)-based 2D perovskites suffer from poor intrinsic stability due to oxidation of $Sn^{2+}$ to $Sn^{4+}$ and hydrolysis reactions with moisture.[30] Interestingly, the introduction of STm ligand into Sn (II)-based 2D perovskite significantly improved the perovskite stability under ambient conditions (~20 °C and ~50% relative humidity). $(STm)_2SnI_4$ thin film can remain high crystallinity (Fig. S3), strong photoluminescence (Fig. S4), and absorption (Fig. S5) over long-time exposure in air. $(STm)_2SnI_4$ exhibits enhanced stability because the π-conjugated STm molecule is bulky and hydrophobic, which serves as an internal encapsulation to the inorganic layer to prevent the air and moisture penetration. Thus, the $Sn^{2+}$ oxidation and hydrolysis reactions are less likely to occur in $(STm)_2SnI_4$. When compared with benchmark $(4Tm)_2SnI_4$ perovskite (Fig. S6), the evolution of full width at half maximum (FWHM) (Fig. S7) and relative intensities (Fig. S8) in XRD over time for $(STm)_2SnI_4$ exhibits similar results, confirming the enhanced stability with the help of STm ligand.

The introduction of STm ligand into Sn (II)-based 2D perovskite can fine-tune the electronic properties as well as material stability, making $(STm)_2SnI_4$ perovskite a good candidate for electronic and optoelectronic applications. Here, FETs with a simple bottom-gate/top-contact (BG-TC) device architecture based on $(STm)_2SnI_4$ thin films were fabricated. Fig. 3 shows the device structure and typical transfer and output characteristics of the devices. A *p*-type transport behaviour was observed with a maximum hole mobility ($\mu_h$) of 1.52 $cm^2 V^{-1}s^{-1}$ (with an average value of up to 1.35 $cm^2 V^{-1} s^{-1}$, which was calculated based on more than 10 devices), which is comparable to the reference $(4Tm)_2SnI_4$ FET devices (Fig. S9). According to the cyclic voltammetry and optical absorption

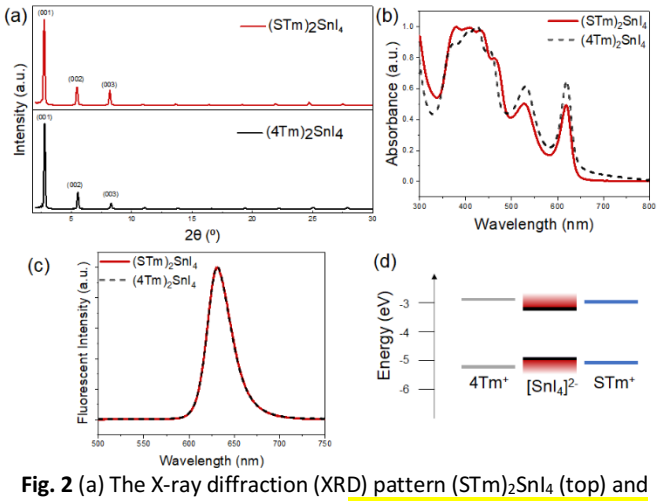


**Fig. 2** (a) The X-ray diffraction (XRD) pattern $(STm)_2SnI_4$ (top) and $(4Tm)_2SnI_4$ (bottom) thin films. (b) UV-vis absorption and (c) photoluminescence spectra of $(STm)_2SnI_4$ and $(4Tm)_2SnI_4$ thin films. (d) Schematic of relative band alignment of STm, 4Tm organic ligands and inorganic $[SnI_4]^{2-}$ layers within 2D hybrid perovskites. The LUMO levels of STm and 4Tm ligands were estimated from HOMO level and optical band gap.

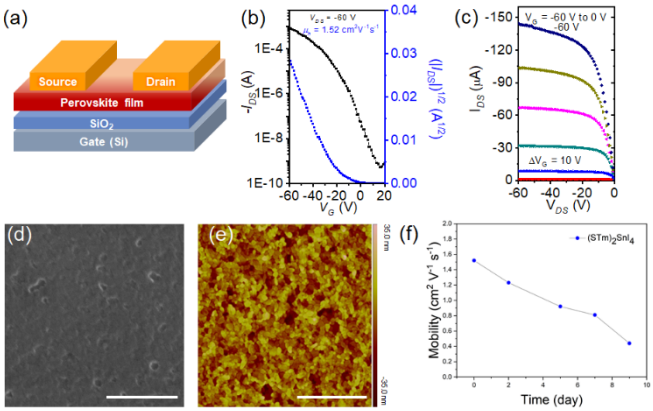


**Fig 3** (a) Device structure and representative transfer (b) and output (c) characteristic of FET devices based on $(STm)_2SnI_4$. SEM image (d) and AFM height image (e) of $(STm)_2SnI_4$ thin films spin-coated on highly n-doped silicon wafers. The scale bars are 2 μm. (f) Evolution of hole mobility of $(STm)_2SnI_4$ FET devices over time.

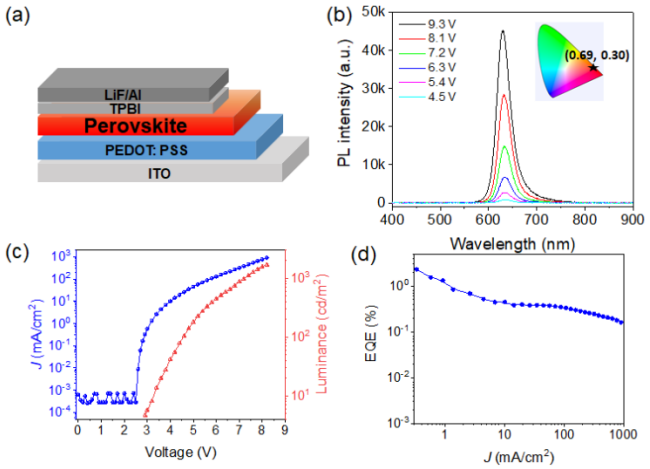


**Fig. 4** (a) LED device structure based on $(STm)_2SnI_4$ perovskite. (b) EL spectra under forward biases of 4.5, 5.4, 6.3, 7.2, 8.1 and 9.3 V. Inset is the CIE coordinate of $(STm)_2SnI_4$ perovskite. (c) current density-voltage-luminance curves and EQE characteristic (d) of champion LED device based on $(STm)_2SnI_4$ hybrid perovskite.

measurement, the HOMO level of STm ligand (-5.05 eV) is shallower than that of 4Tm ligand (-5.12 eV), which could suggest that the incorporation of STm ligand should facilitate better hole injection from gold to the perovskite layers (-5.0 eV) to improve the FET device performances. However, compared with $(4Tm)_2SnI_4$, no obvious enhancement was observed with $(STm)_2SnI_4$-based FET devices even after systematic optimizations on annealing temperatures (Fig. S10). Scanning electron microscope (SEM) (Fig. 3d) and atomic force microscopy (AFM) (Fig. 3e) images shows that the $(STm)_2SnI_4$ thin film has much smaller crystal grains and more grain boundaries than reported $(4Tm)_2SnI_4$-based thin films,[21] with an average grain size of only 0.2 μm. The smaller grain size in $(STm)_2SnI_4$ could inhibit charge transport between crystal grains, leading to a lightly lower hole mobility compared with $(4Tm)_2SnI_4$ FET devices. Nevertheless, the FET performance of $(STm)_2SnI_4$ is indeed better than the conventional 2D perovskite $(PEA)_2SnI_4$ under the same fabrication and characterization conditions.[21]

Additionally, the incorporation of STm ligand into Sn (II)-based 2D perovskite FETs yielded stable devices under ambient conditions. As shown in Fig. 3f, the hole mobility of $(STm)_2SnI_4$ FET devices was well maintained after stored in the air for over nine days without any encapsulations. The conjugated STm ligand significantly protects the $[SnI_4]^{2-}$ octahedron layer from air and moisture penetration so that the charge transport can be efficient, and the field-effect behaviour can be well maintained.

Meanwhile, since the $(STm)_2SnI_4$ perovskite forms a type-I hybrid quantum well configuration with a strong PL emission cantered at 630 nm with a solid-state photoluminescence quantum yield (PLQY) near 4% (Fig. S11), it can be considered as a promising candidate for pure red LED devices. Thus, we incorporated $(STm)_2SnI_4$ perovskite into a functional LED device. The device structure is shown in Figure 4a, where TPBI is short for 1,3,5-tris(1-phenyl-1*H*-benzimidazol-2-yl) benzene and ITO is indium thin oxide. The thickness of PEDOT:PSS, perovskite layer and TPBi were around 40, 25, and 80 nm, respectively. The SEM and AFM images of $(STm)_2SnI_4$ perovskite on PEDOT:PSS/ITO surface (Fig. S12) show similar morphology to the film on a silicon substrate (Fig. 3d and 3e), indicating highly crystalline thin film with small grain sizes (<0.2 μm). Fig. 4b displays the electroluminescence (EL) spectra of $(STm)_2SnI_4$ perovskite LED under varied driving voltages. Those spectra were centred at 630 nm with a narrow full-width at half-maximum (FWHM) of 23.8 nm. The corresponding Commission Internationale de l'Eclairage (CIE) coordinates (Inset of Fig. 4b) were determined to be (0.69, 0.30), suggesting a high-purity red emission. When the driving voltage was increased, the central wavelength of the EL spectra remained unchanged, indicating the colour stability of the LED device. Based on the current density-voltage-luminance (*J-V-L*) curve (Fig. 4c) and EQE characteristic (Fig. 4d) of the champion LED device, a maximum luminance of 1681 cd $m^{-2}$ at 8.2 V and EQE up to 2.28% were achieved, showing a 44% enhancement on EQE compared to $(4Tm)_2SnI_4$ based LED devices.[22] The film optimization based on different perovskite layer annealing temperatures and corresponding device characterizations can be found in Fig. S14. The LED device stability was also examined by measuring the luminance over time at constant current densities (Fig. S15). The $(STm)_2SnI_4$-based LED exhibits outstanding operational lifetimes as $T_{50}$ = 233 min at 100 mA $cm^{-2}$ and $T_{50}$ = 2300 min (~30 h) at 10 mA $cm^{-2}$, which is among the best reported perovskite LEDs.[31, 32]

The improved EQE can possibly be ascribed to two aspects. First, it is proved that in 2D perovskite the decrease of LUMO energy level and increase of HOMO energy level of organic cations can be beneficial for charge transport.[22, 33] The shallower HOMO level of STm ligand make the charge injection from ligand to inorganic perovskite layer charge transport more efficient. In addition, the morphology studies of $(STm)_2SnI_4$ and $(4Tm)_2SnI_4$ thin films reveal that much smaller grain sizes are observed on $(STm)_2SnI_4$ thin films. Small perovskite grain sizes could spatially confine electron and holes to promote radiative recombination.[34, 35] Thus $(STm)_2SnI_4$ with reduced grain sizes is more favourable for LED applications while $(4Tm)_2SnI_4$ with large grain sizes is more suitable for FET applications.

In summary, a novel selenophene-containing conjugated organic ligand has been synthesized and incorporated into Sn (II)-based 2D perovskite. Highly crystalline thin films with strong PL emissions were obtained. Stable and operational FET and LED devices based on $(STm)_2SnI_4$ thin films were fabricated and $(STm)_2SnI_4$-based LED

device shows a 44% improvement than the benchmark $(4Tm)_2SnI_4$-based LED devices. According to thin film optoelectronic property characterizations and morphology studies, the enhancement of $(STm)_2SnI_4$ LED performance is attributed to better band alignment between the organic ligand and the inorganic perovskite layer as well as a more ideal morphology. To the best of our knowledge, this work presents the first study of incorporating selenophene into conjugated organic ligand for 2D perovskite. This work opens up possibilities of introducing heavy atom-based heterocycles into conjugated organic ligands for low-dimensional perovskites.

The materials synthesis work was supported by the US Office of Naval Research under award no. N00014-19-1-2296 (Program Manager: Dr. Joe Parker). Device characterization work was supported by National Science Foundation under award no. 2013644-ECCS.

L.D. conceived the idea and supervised the project. Z.W. carried out the materials synthesis, characterizations, and data analysis. K.W. carried out the LED device fabrications, measurements, and data analysis. W.Z. and Y.G. carried out the FET device fabrications, measurements, and data analysis. Y.G. performed AFM characterizations, provided insightful discussions, and participated in data analysis and manuscript preparation. Q.H. performed SEM characterizations. K.C. carried out cyclic voltammetry measurements. Z.W. and L.D. wrote the manuscript. All authors discussed the results and revised the manuscript.

## Conflicts of interest

There are no conflicts to declare.

## Notes and references

1. B. Saparov and D. B. Mitzi, *Chem. Rev.*, 2016, **116**, 4558-4596.
2. E. Shi, Y. Gao, B. P. Finkenauer, Akriti, A. H. Coffey and L. Dou, *Chem. Soc. Rev.*, 2018, **47**, 6046-6072.
3. K. Zhu, Z. Cheng, S. Rangan, M. Cotlet, J. Du, L. Kasaei, S. J. Teat, W. Liu, Y. Chen, L. C. Feldman, D. M. O'Carroll and J. Li, *ACS Energy Lett.*, 2021, **6**, 2565-2574.
4. J. Xue, R. Wang, X. Chen, C. Yao, X. Jin, K.-L. Wang, W. Huang, T. Huang, Y. Zhao, Y. Zhai, D. Meng, S. Tan, R. Liu, Z.-K. Wang, C. Zhu, K. Zhu, M. C. Beard, Y. Yan and Y. Yang, *Science*, 2021, **371**, 636-640.
5. L. N. Quan, B. P. Rand, R. H. Friend, S. G. Mhaisalkar, T.-W. Lee and E. H. Sargent, *Chem. Rev.*, 2019, **119**, 7444-7477.
6. H.-H. Fang, R. Raissa, M. Abdu-Aguye, S. Adjokatse, G. R. Blake, J. Even and M. A. Loi, *Adv. Funct. Mater.*, 2015, **25**, 2378-2385.
7. M. A. Green, A. Ho-Baillie and H. J. Snaith, *Nat. Photonics*, 2014, **8**, 506-514.
8. Y. Cao, N. Wang, H. Tian, J. Guo, Y. Wei, H. Chen, Y. Miao, W. Zou, K. Pan, Y. He, H. Cao, Y. Ke, M. Xu, Y. Wang, M. Yang, K. Du, Z. Fu, D. Kong, D. Dai, Y. Jin, G. Li, H. Li, Q. Peng, J. Wang and W. Huang, *Nature*, 2018, **562**, 249-253.
9. H. Wang, C. C. S. Chan, M. Chu, J. Xie, S. Zhao, X. Guo, Q. Miao, K. S. Wong, K. Yan and J. Xu, *Sol. RRL*, 2020, **4**, 1900578.
10. H. Zhu, A. Liu, K. I. Shim, J. Hong, J. W. Han and Y.-Y. Noh, *Adv. Mater.*, 2020, **32**, 2002717.
11. X. Li, J. M. Hoffman and M. G. Kanatzidis, *Chem. Rev.*, 2021, **121**, 2230-2291.
12. J. Hu, I. W. H. Oswald, S. J. Stuard, M. M. Nahid, N. Zhou, O. F. Williams, Z. Guo, L. Yan, H. Hu, Z. Chen, X. Xiao, Y. Lin, Z. Yang, J. Huang, A. M. Moran, H. Ade, J. R. Neilson and W. You, *Nat. Commun*, 2019, **10**, 1276.
13. R. Lyu, C. E. Moore, T. Liu, Y. Yu and Y. Wu, *J. Am. Chem. Soc.*, 2021, DOI: 10.1021/jacs.1c05441.
14. Akriti, E. Shi, S. B. Shiring, J. Yang, C. L. Atencio-Martinez, B. Yuan, X. Hu, Y. Gao, B. P. Finkenauer, A. J. Pistone, Y. Yu, P. Liao, B. M. Savoie and L. Dou, *Nat. Nanotechnol*, 2021, **16**, 584-591.
15. D. B. Mitzi, K. Chondroudis and C. R. Kagan, *Inorg. Chem.*, 1999, **38**, 6246-6256.
16. X.-H. Zhu, N. Mercier, P. Frère, P. Blanchard, J. Roncali, M. Allain, C. Pasquier and A. Riou, *Inorg. Chem.*, 2003, **42**, 5330-5339.
17. F. Zhang, H. Lu, J. Tong, J. J. Berry, M. C. Beard and K. Zhu, *Energy Environ. Sci.*, 2020, Medium: ED; Size: p. 1154-1186.
18. C. Ortiz-Cervantes, P. I. Román-Román, J. Vazquez-Chavez, M. Hernández-Rodríguez and D. Solis-Ibarra, *Angew. Chem. Int. Ed.*, 2018, **57**, 13882-13886.
19. I.-H. Park, L. Chu, K. Leng, Y. F. Choy, W. Liu, I. Abdelwahab, Z. Zhu, Z. Ma, W. Chen, Q.-H. Xu, G. Eda and K. P. Loh, *Adv. Funct. Mater.*, 2019, **29**, 1904810.
20. Y. Gao, E. Shi, S. Deng, S. B. Shiring, J. M. Snaider, C. Liang, B. Yuan, R. Song, S. M. Janke, A. Liebman-Peláez, P. Yoo, M. Zeller, B. W. Boudouris, P. Liao, C. Zhu, V. Blum, Y. Yu, B. M. Savoie, L. Huang and L. Dou, *Nat. Chem.*, 2019, **11**, 1151-1157.
21. Y. Gao, Z. Wei, P. Yoo, E. Shi, M. Zeller, C. Zhu, P. Liao and L. Dou, *J. Am. Chem. Soc.*, 2019, **141**, 15577-15585.
22. K. Wang, L. Jin, Y. Gao, A. Liang, B. P. Finkenauer, W. Zhao, Z. Wei, C. Zhu, T.-F. Guo, L. Huang and L. Dou, *ACS Nano*, 2021, **15**, 6316-6325.
23. A. J. Kronemeijer, E. Gili, M. Shahid, J. Rivnay, A. Salleo, M. Heeney and H. Sirringhaus, *Adv Mater*, 2012, **24**, 1558-1565.
24. M. Shahid, T. McCarthy-Ward, J. Labram, S. Rossbauer, E. B. Domingo, S. E. Watkins, N. Stingelin, T. D. Anthopoulos and M. Heeney, *Chem. Sci*, 2012, **3**, 181-185.
25. S. M. Lee, H. R. Lee, G. K. Dutta, J. Lee, J. H. Oh and C. Yang, *Polym. Chem.*, 2019, **10**, 2854-2862.
26. L. Dou, W.-H. Chang, J. Gao, C.-C. Chen, J. You and Y. Yang, *Adv. Mater.*, 2013, **25**, 825-831.
27. H. A. Saadeh, L. Lu, F. He, J. E. Bullock, W. Wang, B. Carsten and L. Yu, *ACS Macro Lett.*, 2012, **1**, 361-365.
28. D. Gao, J. Hollinger, A. A. Jahnke and D. S. Seferos, *J. Mater. Chem. A*, 2014, **2**, 6058-6063.
29. D. Meng, D. Sun, C. Zhong, T. Liu, B. Fan, L. Huo, Y. Li, W. Jiang, H. Choi, T. Kim, J. Y. Kim, Y. Sun, Z. Wang and A. J. Heeger, *J. Am. Chem. Soc.*, 2016, **138**, 375-380.
30. Y. M. Lee, J. Park, B. D. Yu, S. Hong, M. C. Jung and M. Nakamura, *The journal of physical chemistry letters*, 2018, **9**, 2293-2297.
31. K. Lin, J. Xing, L. N. Quan, F. P. G. de Arquer, X. Gong, J. Lu, L. Xie, W. Zhao, D. Zhang, C. Yan, W. Li, X. Liu, Y. Lu, J. Kirman, E. H. Sargent, Q. Xiong and Z. Wei, *Nature*, 2018, **562**, 245-248.
32. H. Wang, F. U. Kosasih, H. Yu, G. Zheng, J. Zhang, G. Pozina, Y. Liu, C. Bao, Z. Hu, X. Liu, L. Kobera, S. Abbrent, J. Brus, Y. Jin, M. Fahlman, R. H. Friend, C. Ducati, X.-K. Liu and F. Gao, *Nat. Commun*, 2020, **11**, 891.
33. J. V. Passarelli, D. J. Fairfield, N. A. Sather, M. P. Hendricks, H. Sai, C. L. Stern and S. I. Stupp, *J. Am. Chem. Soc.*, 2018, **140**, 7313-7323.
34. Z. Xiao, R. A. Kerner, L. Zhao, N. L. Tran, K. M. Lee, T.-W. Koh, G. D. Scholes and B. P. Rand, *Nat. Photonics*, 2017, **11**, 108-115.
35. A. Liang, K. Wang, Y. Gao, B. P. Finkenauer, C. Zhu, L. Jin, L. Huang and L. Dou, *Angew. Chem. Int. Ed.*, 2021, **60**, 8337-8343.

 